




DATE LIST

Contrasting paired benthic and planktonic foraminifera radiocarbon ages from Bermuda Rise ODP Site 1063 during Heinrich Stadials 1 and 2

Jörg Lippold¹ , Jens Fohlmeister^{2,3}, Lukas Wacker⁴ , Michal Kucera⁵, Bernd Kromer^{3,6} and Jens Grützner⁷ 

¹Institute of Earth Sciences, Heidelberg University, Heidelberg, Germany, ²Federal Office for Radiation Protection, Berlin, Berlin, Germany, ³Institute for Environmental Physics, Heidelberg University, Heidelberg, Germany, ⁴Laboratory of Ion Beam Physics, ETH Zurich, Zurich, Switzerland, ⁵MARUM Center for Marine Environmental Sciences, University of Bremen, Bremen, Germany, ⁶Curt-Engelhorn-Zentrum Archäometrie gGmbH, Mannheim, Germany and ⁷Alfred Wegener Institute, Helmholtz-Zentrum für Polar- und Meeresforschung, Bremerhaven, Germany

Corresponding author: Jörg Lippold; Email: joerg.lippold@geow.uni-heidelberg.de

Received: 09 September 2022; **Revised:** 26 May 2024; **Accepted:** 30 May 2024

Keywords: Heinrich events; Last Glacial Maximum; Marine Isotopic Stage 3; North Atlantic; ventilation ¹⁴C ages

Abstract

We report 27 planktonic and 21 benthic radiocarbon ages from the subtropical marine sediment core ODP Site 1063 (Bermuda Rise) for the time range between 30 and 14 ka before present. Despite low abundances of benthic specimens, it was possible to measure radiocarbon ages down to ~10 µg carbon using a MICADAS and the gas ion source developed at ETH Zurich. Based on a tentative radiocarbon-independent age-model we found that the radiocarbon reservoir of the bottom water varied moderately relative to the analytical and age-model related uncertainties throughout the examined time-period, but larger differences in the radiocarbon reservoir appear to have affected the upper ocean layer. In particular, radiocarbon levels around Heinrich Stadial 2 reveal surface radiocarbon content similar to that of the atmosphere, while during Heinrich Stadial 1 surface waters were significantly depleted in ¹⁴C.

Introduction

Ocean Drilling Program (ODP) Site 1063 (33°41'N, 57°37'W) was drilled during ODP Leg 172 at a water depth of 4,584 m (Keigwin et al. 1998) at the Bermuda Rise. The sediment drifts of the Bermuda Rise represent a high-resolution archive of paleoclimatic and paleoceanographic information. Due to sedimentation rates partly exceeding 150 cm/kyr during glacials (Channell et al. 2012) and because the site is bathed by the deepest water masses of the North Atlantic, this region has been intensively studied in particular in terms of reconstructing late Pleistocene deep-water mass geometry and the strength of the Atlantic Meridional Overturning Circulation (Böhm et al. 2015; Deaney et al. 2017; Gutjahr and Lippold, 2011; Henry et al. 2016; Jaume-Seguí et al. 2020; Keigwin and Boyle, 2008; Keigwin and Boyle, 2000; Lippold et al. 2009; Lippold et al. 2019; McManus et al. 2004; Roberts et al. 2010), while paleoceanographic reconstructions from this core location are repeatedly under discussion given the presence of benthic nepheloid layers (Lerner et al. 2019) and indications for high levels of bioturbation at this drift deposit site (Çağatay et al. 2001).

We carried out ¹⁴C measurements from co-existing planktonic and benthic foraminifera covering the time period between 30 and 14 ka before present (BP) to examine radiocarbon surface and bottom reservoir effects and to derive the ventilation age of the deep-water masses in the NW Atlantic since the Marine isotopic Stage 3 (MIS3).

Methods

Sediment samples

The examined 27 samples from ODP Site 1063 (Holes B and D) cover the interval from 2.13 to 14.62 meters of composite depth, which previous age models indicated to encompass the time period across Heinrich Events 2 and 1 (Keigwin et al. 1998, 2005). Prior to sampling, depth correlation between Hole D (22 samples) and Hole B (5 samples) has been refined by aligning high resolution magnetic susceptibility records from both holes (Keigwin et al. 2005), such that the selected samples covered the target interval evenly in age. Due to the high sedimentation rate, where accumulated material predominantly contains clays, silts, and nannofossils, and the water depth close to the regional lysocline, only small amounts of carbonate material were available in each sample and we therefore requested large samples, covering 2-cm core slices for analyses. Foraminifera were extracted from the sediment using standard methods (disintegration of sediment in de-ionized water followed by washing over a 0.063 mm sieve and manual picking from the dry-sieved 0.150 mm residue) at the Department for Geosciences, University of Tübingen. For the analysis of surface water radiocarbon ages, monospecific aliquots of the only sufficiently abundant planktonic foraminifera (*Globorotalia inflata*) were obtained. Other surface dwellers, such as *Globigerinoides ruber* or *Trilobatus sacculifer*, occurred in too low abundance only. For the analysis of deep-water radiocarbon ages, assemblages of mixed benthic species (including epifaunal and infaunal species) were sampled and separated. Sample masses of the planktonic foraminifera were between 4 and 37 mg, while benthic samples always yielded less than 1 mg (Table 1).

AMS

All planktonic foraminifera samples with more than 5 mg were prepared for conventional radiocarbon AMS measurements with solid C targets. The samples were dissolved in 3N HCl under vacuum and dried in a water trap using a dry-ice acetone mixture. The remaining pure CO₂ gas is captured with liquid nitrogen and attached to the graphitisation line. Here, the CO₂ reacts with H₂ to C and H₂O at 575°C using an iron catalyst (Alfa Aesar, -325 mesh). The solid C samples were measured at the Klaus Tschira Laboratory for scientific dating (Kromer et al. 2013) against the Oxalic Acid II standard and blank values derived from approximately ~200 ka old foraminifera from the same marine sediment core. Benthic foraminifera were much less abundant yielding amounts of less than 1 mg CaCO₃. Therefore, to determine the radiocarbon content in the scarce benthic species in addition to the contemporaneous planktonic samples, we measured the ¹⁴C content of CO₂ evolved from the carbonate and directly introduced it to the gas ion source as developed at the AMS lab in Zurich (Wacker et al. 2013a). This method allows analyses using as little as 100–600 µg of carbonate (about 10–60 µg C). A sample of 400 µg carbonate (40 µg C) gives typically a ¹⁴C- current of 10–15 µA over 20 minutes and yields a measurement precision of less than 7‰ for a modern sample (Wacker et al. 2013b). All samples were measured against the Oxalic Acid II standard accompanied by measurements of ¹⁴C-free ~200 ka old foraminifera from the same sediment core for blank corrections. Using the gas ion source allows to measure radiocarbon in the CO₂ phase and reduces the risk of contamination during sample handling in the conventional AMS method. Nevertheless, measurement errors are generally larger due to the limited sample mass and the reduced ionization probability using the gas ion source compared to the solid target technique. The applicability of the gas ion source has been well addressed in several studies, which compared results of solid targets and the gas ion source of identical carbonate samples (Bard et al. 2015; Gottschalk et al. 2018; Molnár et al. 2021; Wacker et al. 2013a).

Table 1. Samples, core depth, sample weight, radiocarbon results and age of foraminifera from ODP Site 1063

Hole	Core section	Depth in section (cm)	Meter composite depth (mcd)	Planktonic				Benthic					NGRIP aligned age (ka BP) (Figure 1)		
				Lab #	<i>G. inflata</i> (mg CaCO ₃)	¹⁴ C age (¹⁴ C yr BP)	Error 1σ	Lab #	Mixed benthos (mg CaCO ₃)	¹⁴ C age (¹⁴ C yr BP)	Error 1σ	Comment		B-P age (¹⁴ C yr BP)	Error 1σ
D	1H2W	35–37	2.13	MAMS16199	32.16	13,170	50	ETH 44161	0.45	14,910	160		1740	170	14.8
D	1H2W	55–57	2.33	MAMS16200	28.14	13,380	50	ETH 44162	0.32	14,330	170		950	180	15.1
B	1H2W	93–95	2.63	MAMS16201	37.29	14,230	50	ETH 44163	0.23	14,560	220		330	220	15.6
B	1H2W	103–105	2.73	MAMS15409	11.22	14,670	50	ETH 44164	0.32	16,180	230		1510	240	15.8
B	1H2W	127–129	2.97	MAMS13958	8.40	14,830	70	ETH 44148	0.13	15,880	200	Small sample size	1050	210	16.1
B	1H3W	11.5–13.5	3.32	MAMS13959	15.70	14,960	60	ETH 44149	0.18	16,630	220		1670	230	16.3
B	1H3W	107–109	4.27	MAMS13960	5.68	16,500	70	ETH 44150	0.17	17,290	240		790	250	16.9
D	2H1W	131–133	4.99	MAMS15410	11.23	17,050	60	ETH 44165	0.26	16,930	250		–120	260	17.4
D	2H2W	76–78	5.94	MAMS15411	5.69	17,900	70								18.4
B	1H5W	22.5–24.5	6.43	ETH 44158	4.60	17,800	210								19.0
D	2H3W	56–58	7.24	MAMS15412	4.22	18,580	80								20.2
D	2H3W	95–97	7.58	ETH 44159	3.20	18,620	220	ETH 44152	0.77	20,010	250		1390	330	20.6
D	2H4W	55–57	8.73	MAMS15413	7.42	19,070	70								22.2
D	2H4W	104–106	9.22	MAMS15414	19.06	19,940	80	ETH 44169	0.11	21,380	550	Small sample size	1440	560	22.9
D	2H5W	4–6	9.72	MAMS15415	11.21	20,410	80								23.6
D	2H5W	54–56	10.22	MAMS16202	4.60	20,600	80								24.3
D	2H5W	76–78	10.44	MAMS16209	5.39	20,900	80	ETH 44172	0.22	22,740	340		1840	350	24.6
D	2H5W	111–113	10.79	MAMS15416	6.18	21,450	100	ETH 44173	0.23	22,820	370		1370	380	25.1
D	2H6W	34–36	11.52	ETH 44160	4.10	21,480	240	ETH 44153	0.34	26,480	420		5000	480	26.1
D	2H6W	44–46	11.62	MAMS15417	3.60	21,530	100	ETH 44174	0.22	23,440	500		1910	510	26.3
D	2H6W	99–101	12.17	MAMS16204	12.66	22,210	80	ETH 44175	0.17	23,660	500		1450	510	26.8
D	3H1W	79–81	12.91	MAMS15418	3.70	22,790	110	ETH 44176	0.09	26,390	900	Small sample size	3600	910	27.4
D	2H7W	50–52	13.17	MAMS13964	12.10	23,680	130	ETH 44154	0.15	25,090	450		1410	470	27.6
D	3H2W	16–18	13.78	MAMS16205	14.15	24,670	110	ETH 44177	0.21	26,380	600		1710	610	28.4
D	3H2W	51–53	14.13	MAMS15419	10.67	25,800	150	ETH 44178	0.23	26,340	600		540	620	28.90
D	3H2W	71–73	14.33	ETH 44186	5.91	26,400	390	ETH 44179	0.21	26,960	600		560	720	29.3
D	3H2W	100–102	14.62	MAMS13965	7.78	26,260	180	ETH 44155	0.33	27,700	500		1440	530	30.0

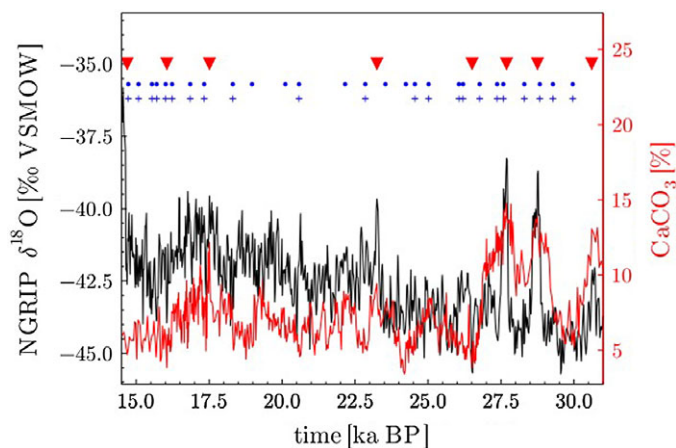


Figure 1. Alignment of the CaCO_3 profile from ODP site 1063 (Keigwin et al. 2005) to the $\delta^{18}\text{O}$ profile of the NGRIP ice core (Andersen et al. 2004). Red triangles denote position of tie points used for the age-model tuning. Blue symbols indicate positions of ^{14}C -measurements of benthic (crosses) and planktonic (circles) foraminifera for this study.

Tentative ^{14}C -independent age model

We refined the available age model for ODP Site 1063 for the examined time period (Böhm et al. 2015; Grützner et al. 2002) by tuning XRF derived CaCO_3 content of the sediment to the $\delta^{18}\text{O}$ signal of Greenland NGRIP ice core (Andersen et al. 2004). As both records reflect a Daansgard/Oeschger event (DO) like behaviour in their signals with the ice core being well dated in the period of interest by annual layer counting, we use the prominent DO pattern to derive an absolute age for ODP Site 1063. We identified DO events between 40 and 15 ka BP in ODP Site 1063 sediment properties, allowing a millennial-resolution age tuning. For the time interval between 36 and 10 ka we identified 12 tuning points, hence one tuning point per approximately 2200 a (Figure 1, Table 2). We set the tuning points preferentially to the start and end-points of DO-events, and thus mark identical time stamps in both records, on which the tuning is based. Here, we assume, that there is no significant lag in the CaCO_3 content of ODP Site 1063 compared to the $\delta^{18}\text{O}$ signal from NGRIP (Buizert et al. 2015), as fine scale variations (< 200 a) are recorded consistently in both archives. In order to improve our decision in setting the tuning points, we applied a Monte Carlo algorithm (Fohlmeister, 2012), which varies all tuning points within its given uncertainties to maximize the correlation between the ice core data and the elemental composition of the sediment core. Thus, we assume an age error of 0.2 ka for the absolute ages, i.e. the subjectively chosen tie points where optimised by an objective statistical method. The assumed age error of 0.2 ka is accounted for in the resulting radiocarbon reservoir ages (in addition to the ^{14}C analytical uncertainties). Even if the variations in NGRIP $\delta^{18}\text{O}$ and ODP Site 1063 CaCO_3 content did not occur simultaneously, a potential lagging mechanism must have been rather constant and small as the shape of the DO events is maintained during the sedimentation process, potentially resulting only in minor reservoir age offsets. Nonetheless, we note that the alignment of the variations in sedimentary CaCO_3 to the $\delta^{18}\text{O}$ of NGRIP is based on the assignment of wiggles and may therefore represent only one out of other possible age-depth realisations.

Results

We report 27 planktonic and 21 benthic radiocarbon ages and thus 21 benthic-planktonic (B-P) ventilation ages from ODP Site 1063 in the time range between 30 and 14 ka BP (Table 1).

Table 2. List of used tie points for the age model construction

NGRIP derived age (ka BP)	Age error (ka)	ODP 1063 core depth (mcd)
11.76	0.2	1.58
14.74	0.2	2.12
16.10	0.2	2.86
17.56	0.2	5.46
23.3	0.2	9.50
26.56	0.2	11.86
27.74	0.2	13.34
28.80	0.2	14.04
30.66	0.2	14.96
32.48	0.2	15.52
33.68	0.2	15.96
35.44	0.2	16.44
38.20	0.2	17.28
40.12	0.2	18.06

The B-P ages in our study vary from a range between -120 to 5000 ^{14}C -years with an average of 1500 . The bulk of the data falls within a broad band of values between 330 and 1990 ^{14}C -years. The temporal variations within this band might not be subject to fine-scale interpretation given the analytical uncertainties introduced largely by the benthic measurements and the relatively coarse resolution of our ^{14}C samples.

Discussion and conclusions

Deviating from the majority of our data three values stand out with very large (5000 and 3600 ^{14}C -years) or very small (-120 ^{14}C -years) B-P ages. Both the small negative B-P age around 17.4 ka BP (close to the onset of Heinrich Stadial 1), which would suggest the same water mass origin for the near-surface and the bottom water at this site, and the old B-P ages at 26.1 and 27.4 ka BP (before Heinrich Stadial 2), potentially indicating near-surface and bottom water masses of very different origin, are not reflected by the surrounding B-P ages of our record. We cannot exclude the possibility that such features might have been introduced by bioturbation or transport of allochthonous tests albeit the high sedimentation rate (on average ~ 90 cm/ka) suggests this process to have a limited effect throughout the core. In particular, the three observed very high or very low B-P ages are not exclusively associated with high or low sedimentation rates. In support of these more extreme values representing real B-P differences, there is ^{14}C -based evidence for similar fast and strong ventilation changes from various other Atlantic bottom water locations (e.g., data compilation by Rafter et al. 2022) within the time range between 25 and 15 ka BP.

Based on our tentative ^{14}C -independent age model we calculated the radiocarbon surface reservoir age by comparing the ^{14}C results of the planktonic species with the contemporaneous atmospheric value for the (^{14}C -independent) site-specific chronology. The radiocarbon surface reservoir is a measure for the interaction of old deep-water masses with water at the surface or the intensification of exchange between deep and surface waters. In addition, we calculated the radiocarbon difference between the benthic foraminifera and atmospheric values. The benthic radiocarbon offset gives an information on how long the deep water mass was separated from the atmosphere (Skinner and Bard 2022). When considering the analytical uncertainties and assuming that our ^{14}C -independent age model is correct, we found that based on our benthic results the radiocarbon reservoir of the bottom water was on average 2400 ± 800 ^{14}C -years and varied little throughout the examined time-period. In contrast, derived from the planktonic data we found larger relative differences in the radiocarbon reservoir at the surface (1040 ± 910 ^{14}C -years, Table 2, Figure 2). In particular, surface water radiocarbon levels around

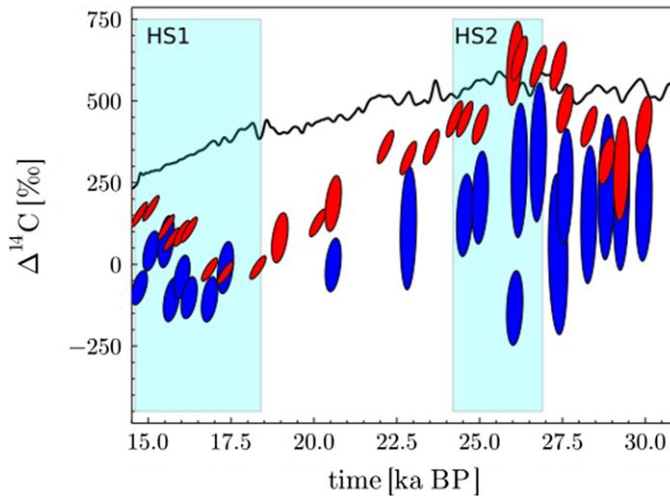


Figure 2. Decay-corrected ($\Delta^{14}\text{C}$) for the atmosphere (black solid line, *IntCal2020; Reimer et al. 2020*) in comparison with the radiocarbon content measured in planktonic (red ellipses) and benthic (blue ellipses) foraminifera. Error ellipses denote 95% confidence intervals. Cyan rectangles denote the approximate timing of Heinrich Stadials 1 and 2 as derived from peaks in sedimentary $^{231}\text{Pa}/^{230}\text{Th}$ from the Bermuda Rise (*Lippold et al. 2009; McManus et al. 2004*).

Heinrich Stadial 2 nearly reach those of the atmosphere, whereas during Heinrich Stadial 1 the surface waters were significantly depleted in ^{14}C . These differences between both prominent Northern Hemisphere cold events require further research (*Bauska et al. 2021; Shuttleworth et al. 2021*), since deep ocean circulation proxies (e.g. $^{231}\text{Pa}/^{230}\text{Th}$, ϵNd) indicate similar conditions for both cold events (*Gutjahr and Lippold 2011; Lippold et al. 2009; McManus et al. 2004; Roberts et al. 2010*). Surface water radiocarbon content around Heinrich Stadial 2 indicates a good ventilation and equilibration of surface waters with the atmosphere. This implies a relatively strong stratification of surface waters preventing old, carbon rich bottom waters from upwelling. In contrast to Heinrich Stadial 2, Heinrich Stadial 1 surface waters seem not to have experienced such stratification. The high variability of the B-P ages at ODP Site 1063 and the deviating observations for Heinrich Stadial 2 and 1 are not in agreement with interpretation of other paleocirculation observations from the Bermuda Rise (*Gutjahr and Lippold 2011; Lippold et al. 2009; McManus et al. 2004; Roberts et al. 2010*) and might be related not purely to oceanographic explanations. It is possible that the planktonic signal may not represent the surface mixed layer, because the analysed planktonic species *G. inflata* is known to add a significant portion of the shell calcite within the thermocline (*van Raden et al. 2011*). However, it is unlikely that the depth habitat of the species changed significantly between the two Heinrich Events (*Jonkers et al. 2021*). Another process potentially capable of influencing the apparent ^{14}C age of a sediment horizon is bioturbation, in particular during times of variability in the abundances of different species. Bioturbational mixing of tests out of abundance maxima into older or younger sediment layers can result in apparent isotopic gradients between different species (*Löwemark et al. 2008*). However, the high sedimentation rate at this site and the clear manifestation of DO-cycles in the sedimentary record argue against a crucial role of bioturbation.

Nevertheless, this data set reports high variability in radiocarbon levels during the coldest period of the last glacial cycle. This observation may provide helpful information for future studies on past ventilation changes of the Atlantic Ocean.

Acknowledgments. The authors thank the IODP Core Repository in Bremen for providing sample material, Margret Bayer and Hartmut Schulz for support in the lab and Julia Gottschalk for discussions. We thank the Deutsche Forschungsgemeinschaft (DFG) for funding this study via grants FO809/1-1 and LI1815/4-2.

References

- Andersen KK, Azuma N, Barnola JM, Bigler M, Biscaye P, et al. (2004) High-resolution record of Northern Hemisphere climate extending into the last interglacial period. *Nature* **431**(7005), 147–151.
- Bard E, Tuna T, Fagault Y, Bonvalot L, Wacker L, Fahrni S and Synal H-A (2015) AixMICADAS, the accelerator mass spectrometer dedicated to ^{14}C recently installed in Aix-en-Provence, France. *Nuclear Instruments and Methods in Physics Research Section B: Beam Interactions with Materials and Atoms* **361**, 80–86.
- Bauska TK, Marcott SA and Brook EJ (2021) Abrupt changes in the global carbon cycle during the last glacial period. *Nature Geoscience* **14**(2), 91–96.
- Böhm E, Lippold J, Gutjahr M, Frank M, Blaser P, et al. (2015) Strong and deep Atlantic meridional overturning circulation during the last glacial cycle. *Nature* **517**, 73–76.
- Buizert C, Adrian B, Ahn J, Albert M, Alley RB, et al. (2015) Precise inter-polar phasing of abrupt climate change during the last ice age. *Nature* **520**(7549), 661–665.
- Çağatay MN, Borowski WS, Ternois YG (2001) Factors affecting the diagenesis of Quaternary sediments at ODP Leg 172 sites in western North Atlantic: evidence from pore water and sediment geochemistry. *Chemical Geology* **175**, 467–484.
- Channell JET, Hodell DA and Curtis J (2012) ODP Site 1063 (Bermuda Rise) revisited: Oxygen isotopes, excursions and paleointensity in the Brunhes Chron. *Geochemistry Geophysics Geosystems* **13**(1).
- Deaney EL, Barker S and van de Flierdt T (2017) Timing and nature of AMOC recovery across Termination 2 and magnitude of deglacial CO_2 change. *Nature Communications* **8**, 14595.
- Fohlmeister J (2012) A statistical approach to construct composite climate records of dated archives: *Quaternary Geochronology* **14**, 48–56.
- Gottschalk J, Szidat S, Michel E, Mazaud A, Salazar G, et al. (2018) Radiocarbon measurements of small-size foraminiferal samples with the Mini Carbon Dating System (MICADAS) at the University of Bern: implications for paleoclimate reconstructions. *Radiocarbon* **60**(2), 1–23.
- Grützner J, Giosan L, Franz SO, Tiedemann R, Cortijo E, et al. (2002) Astronomical age models for Pleistocene drift sediments from the western North Atlantic (ODP Sites 1055-1063). *Marine Geology* **189**, 5–23.
- Gutjahr M and Lippold J (2011) Early arrival of Southern Source Water in the deep North Atlantic prior to Heinrich event 2. *Paleoceanography* **26**, PA2101.
- Henry LG, McManus JF, Curry WB, Roberts NL, Piotrowski AM and Keigwin LD (2016) North Atlantic ocean circulation and abrupt climate change during the last glaciation. *Science* **353**(6298), 470–474.
- Jaume-Seguí M, Kim J, Pena L, Goldstein S and Knudson K, et al. (2020) Distinguishing Glacial AMOC and Interglacial non-AMOC Nd Isotopic Signals in the Deep Western Atlantic over the last 1 Myr. *Paleoceanography and Paleoclimatology* **12**(12), e2020PA003877.
- Jonkers L, Gopalakrishnan A, Weßel L, Chiessi CM and Groeneveld J, et al. (2021) Morphotype and crust effects on the geochemistry of *Globorotalia inflata*. *Paleoceanography and Paleoclimatology* **36**(4), e2021PA004224.
- Keigwin D and Boyle E (2008) Did North Atlantic overturning halt 17,000 years ago? *Paleoceanography* **23**, PA1101.
- Keigwin L and Boyle E (2000) Detecting Holocene changes in thermohaline circulation. *Proceedings of the National Academy of Sciences* **97**(4), 1343–1346.
- Keigwin L, Rio D, Acton G, et al. (1998) Bermuda Rise and Sohm abyssal plain, Sites 1063 and 1064. *Proceedings of the Ocean Drilling Program, Initial Reports* **172**.
- Keigwin LD, Rio D, Acton GD and Shipboard Scientific (2005) Magnetic susceptibility on ODP Hole 172-1063B. PANGAEA. <https://doi.org/10.1594/PANGAEA.266175>.
- Kromer B, Lindauer S, Synal H-A and Wacker L (2013) MAMS—a new AMS facility at the Curt-Engelhorn-Centre for Achaometry, Mannheim, Germany. *Nuclear Instruments and Methods in Physics Research Section B: Beam Interactions with Materials and Atoms* **294**, 11–13.
- Lerner P, Marchal O, Lam PJ, Gardner W, Richardson MJ, and Mishonov A (2019) A model study of the relative influences of scavenging and circulation on ^{230}Th and ^{231}Pa in the western North Atlantic: Deep Sea Research Part I. *Oceanographic Research Papers* **155**, 103159.
- Lippold J, Grützner J, Winter D, Lahaye Y, Mangini A and Christl M (2009) Does sedimentary $^{231}\text{Pa}/^{230}\text{Th}$ from the Bermuda Rise monitor past Atlantic Meridional Overturning Circulation? *Geophysical Research Letters* **36**, L12601.
- Lippold J, Pöppelmeier F, Süfke F, Gutjahr M, Goepfert TJ, et al. (2019) Constraining the variability of the Atlantic Meridional Overturning Circulation during the Holocene. *Geophysical Research Letters* **46**(20), 11338–11346.
- Löwemark L, Constantinou K and Steinke S (2008) Bias in foraminiferal multispecies reconstructions of paleohydrographic conditions caused by foraminiferal abundance variations and bioturbational mixing: A model approach. *Marine Geology* **256**(1–4), 101–106.
- McManus J, Francois R, Gherardi J, Keigwin L and Brown-Leger S (2004) Collapse and rapid resumption of Atlantic meridional circulation linked to deglacial climate change. *Nature* **428**, 834–837.

- Molnár M, Mészáros M, Janovics R, Major I, Hubay K, et al. (2021) Gas ion source performance of the environmental micADAS at Hekal Laboratory, Debrecen, Hungary. *Radiocarbon* **63**(2), 499–511.
- Rafter PA, Gray WR, Hines SKV, Burke A, Costa KM, et al. (2022) Global reorganization of deep-sea circulation and carbon storage after the last ice age. *Science Advances* **8**(46), eabq5434.
- Reimer PJ, Austin WEN, Bard E, Bayliss A, Blackwell PG, et al. (2020) The IntCal20 Northern Hemisphere radiocarbon age calibration curve (0–55 cal kBP). *Radiocarbon* **62**(4), 725–757.
- Roberts N, Piotrowski A, McManus J and Keigwin L (2010) Synchronous deglacial overturning and water mass source changes. *Science* **327**, 75–78.
- Shuttleworth R, Bostock HC, Chalk TB, Calvo E, Jaccard SL, et al. (2021) Early deglacial CO₂ release from the Sub-Antarctic Atlantic and Pacific oceans. *Earth and Planetary Science Letters* **554**, 116649.
- Skinner LC and Bard E (2022) Radiocarbon as a dating tool and tracer in palaeoceanography. *Reviews of Geophysics* **60**(1).
- van Raden UJ, Groeneveld J, Raitzsch M and Kucera M (2011) Mg/Ca in the planktonic foraminifera *Globorotalia inflata* and *Globigerina bulloides* from Western Mediterranean plankton tow and core top samples. *Marine Micropalaeontology* **78**, 3–4.
- Wacker L, Lippold J, Molnár M and Schulz H (2013a) Towards single-foraminifera-dating with a gas ion source. *Nuclear Instruments and Methods in Physics Research B* **294**, 307–310.
- Wacker LS, Fahrni SM, Hajdas I, Molnár M, Sýnal H-A, Szidat S and Zhang YL (2013b) A versatile gas interface for routine radiocarbon analysis with a gas ion source. *Nuclear Instruments and Methods in Physics Research B* **294**, 315–319.